Investigating the influence of pigmentation on the electrolyte transport properties of organic coatings using ORP-EIS

Madelat, Negin; Wouters, Benny; Visser, Peter; Jiryaeisharahi, Zahra; Marcoen, Kristof; Abrahami, Shohsan T.; Hubin, Annick; Terryn, Herman; Hauffman, Tom

DOI
10.1016/j.corsci.2023.111699

Publication date
2024

Document Version
Final published version

Published in
Corrosion Science

Corrosion Science 227 (2024) 111699

Contents lists available at ScienceDirect

Corrosion Science

journal homepage: www.elsevier.com/locate/corsci

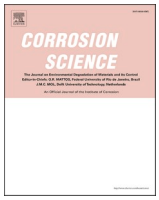

Investigating the influence of pigmentation on the electrolyte transport properties of organic coatings using ORP-EIS

Negin Madelat [a,*], Benny Wouters [a], Peter Visser [b], Zahra Jiryaeisharahi [a], Kristof Marcoen [a], Shoshan T. Abrahami [c], Annick Hubin [a], Herman Terryn [a], Tom Hauffman [a]

[a] Vrije Universiteit Brussel, Research Group Electrochemical and Surface Engineering, Department Materials and Chemistry, Pleinlaan 2, B-1050 Brussels, Belgium
[b] AkzoNobel, Rijksstraatweg 31, 2171AJ Sassenheim, the Netherlands
[c] Delft University of Technology, Department of Materials science and Engineering, Mekelweg 2, 2628 CD Delft, the Netherlands

ARTICLE INFO

Keywords:
Organic coating
ORP-EIS
Water uptake
Ion diffusion
GDOES

ABSTRACT

In this work, the correlation between electrolyte transport properties and the variation of pigment volume concentration (PVC) in a series of organic coatings is explored. Using an odd random phase electrochemical impedance spectroscopy (ORP-EIS) approach, the diffusion of ions independent from water take-up is analysed. A higher PVC resulted in a more homogeneous coating morphology, which could be associated with a faster diffusion of ions following a Fickian regime and enhanced water uptake. In the case of lower pigment loading, the obtained heterogenous morphology of the coating introduced new challenges to the physical interpretation of the proposed electrochemical equivalent circuit.

1. Introduction

Organic coatings are widely applied in corrosion protection practices [1,2]. To satisfy aesthetic requirements and implement desired functions, different additives and in particular pigments are embedded in the coating. The addition of pigments can introduce both advantages and disadvantages to the system. Literature attests the influence of pigmentation on mechanical properties, thermal properties and glass transition temperature, film formation, stress build up and coating/electrolyte interactions [3]. To provide high corrosion resistance, coatings should afford adequate barrier properties against the penetration of corrodents from surrounding environment. Therefore, understanding the influence of pigmentation on the electrolyte transport is crucial, but stays elusive. While polarity and free volume of the polymer matrix are the main factors influencing the water uptake of clearcoats [4–6], the list expands in the presence of pigments. The distinct pigment/polymer interfacial chemistry and the adhesion properties at these interfaces are among the influential factors. Emad et al. have proposed the pigment/binder interfacial zone as a host area for water which facilitates the transport of electrolyte and increases the leaching, leaving cavities for further direct transport properties [7]. Meng et al. have shown that the modification of mica as the incorporated pigment causes slower absorption rate and less water uptake. The decrease in water uptake is associated with the improved compactness of the coating due to the formation of chemical bonds at the pigment/binder interface [8]. The other mechanism proposed for an altered ingress of the electrolyte in the pigmented coating is the stress built up. Lacombre et al. published a series of articles in which they studied the influence of pigmentation in organic coatings through a thermodynamic approach [9–11]. They have correlated the initial faster diffusion of water to the stress built up in the pigmented epoxy samples, increasing the entropy of diffusion. It was shown that with incorporation of 20 wt% TiO_2, the barrier properties of the coating diminish more rapidly in comparison with the clearcoat [9]. Morsch et al. have verified the correlation between stress built up in pigmented coatings and water transport, using microscale polyethylene-coated silica pigment in an epoxy-amine coating. In this study, AFM-IR in combination with thermal analysis confirmed the preferential and random uptake of water through the polymer network rather than the pigment/binder hybrid interphase [12]. Since addition of the pigments to the coating can significantly alter its barrier properties, pigment volume concentration (PVC) becomes an impactful parameter [3,4,13]. Van der Wel et al. have discussed the influence of PVC in two different categories of pigmentation, ideal and non-ideal pigmentation. In ideal pigmentation, the increase in PVC can decrease the diffusion coefficient (D) of water due to the increase in the effective path length. On the other hand, the increase in the volume fraction of

* Corresponding author.
E-mail address: Negin.Madelat@vub.be (N. Madelat).

https://doi.org/10.1016/j.corsci.2023.111699
Received 15 September 2023; Received in revised form 25 October 2023; Accepted 19 November 2023
Available online 22 November 2023
0010-938X/

impermeable pigments decreases the water solubility (S). Therefore, the permeability (P) will decrease with an increase in PVC. The decrease in permeability is restricted by the critical pigment volume concentration (CPVC). Above the CPVC, the permeability increases significantly due to the poor wetting of the pigments and formation of voids. In non-ideal pigmentation, particle flocculation results in the formation of vulnerable interfaces, providing a faster diffusion path than the polymer matrix [4]. One should notice that the true output of this classification depends on a plethora of factors such as type, size, and physicochemical properties of the pigments which needs to be explored in each particular system. Different case studies are reviewed in the work of Perera et al. [3].

As summarized above, water uptake in pigmented coatings has been exploited throughout the years. However, mechanistic insights about the individual diffusion of ions apart from water, its influence on the barrier properties of the coating, and the correlation between the coating morphology/structure and ion diffusion, requires comprehensive studies. In this paper, the goal is to explore the relationship between the separate movement of the ions and water and the morphology of the coating when the PVC changes.

Electrochemical impedance spectroscopy is a widely applied non-destructive technique to investigate the transport properties of organic coatings in situ [14–20]. In this paper, an odd random phase electrochemical impedance spectroscopy (ORP-EIS) approach is employed to investigate the transport properties of different coatings. ORP-EIS has been extensively applied for studies related to coatings, interfaces, batteries and electrochemical purification of metals [21–30]. Using ORP-EIS, the application of a multisine signal shortens the measurement time which effectively decreases the potential influence of non-stationarities on the system. On the other hand, the excitation of only the odd harmonics along with the random omission of 1 out of 3 consecutive harmonics provides valuable information on the standard deviation on the output signals of excited and non-excited odd and even frequencies. This information determines the contribution of different noise levels to the system [31–33]. In presence of non-stationarities, the impedance data can be resolved over time to provide instantaneous impedance data [34,35]. When exposing organic coatings to the electrolyte, initial fast water uptake and its diffusion coefficient as well as the ion diffusion can be studied using instantaneous impedance [23,25].

This work will focus on three different coatings with varying PVCs (10%, 20% and 30%) as well as the clearcoat applied on acidic pickled aluminium substrates. A two-layer electrochemical equivalent circuit (EEC) is used to differentiate between the diffusion of water and ions. This model has proven to be a powerful tool to evaluate the independent ion diffusion using an integrated spectro-electrochemical approach and to explore the contribution of buried interfaces to the general electrochemical state of coated structures in our previous publications [25,28]. In the present study, the combination of ORP-EIS, scanning electron microscopy (SEM) images and glow discharge optical emission spectroscopy (GDOES) depth profiles is used to generate insights about the morphology induced dynamics.

2. Materials and methods

2.1. Sample preparation

AA2024 alloy test panels cladded with a commercially pure aluminium grade (WL 3.1364–1) were degreased with isopropanol followed by 15 min degreasing in an alkaline agent at 60°C. Afterwards, alkaline etching was conducted for 1 min at 60°C. Eventually, acidic pickling was performed in a fluoride containing solution for 5 min at 35°C. After each step (degreasing, etching and acidic pickling), the samples were rinsed in an agitated deionised water bath for 3 min.

The epoxy-amine based coatings were formulated with different PVC levels of 0, 10%, 20% and 30% using pigments and extenders and the naming of the samples are EA-CC, EA-10P, EA-20P and EA-30P, respectively. The critical pigment volume concentration (CPVC) of this blend is 56% and hence the respective PVCs are well below the CPVC. The compositions of the coatings are summarized in Table 1. The coatings were prepared according to the following procedure: the ingredients of component A were added under stirring into a 370 ml glass jar. The pigments were dispersed to a fineness of grind less than 25 μm by shaking, on a Skandex® paint shaker using 400 g of Zirconox® pearls (1.7–2.4 mm) as the grinding medium which was separated from the mixture after the dispersion. Component B (hardener) and component C (thinner) were prepared separately and added to component A under stirring. Hereafter, the substrates were coated with epoxy-amine based coatings using a spray robot, targeting a dry thickness of 30 μm. All samples were applied at ambient conditions at 23 °C and 55% RH. The samples were cured in an oven (1 h at 80 °C) after a 1 h flash-off period. The glass transition temperature (T_g) of the samples was measured using modulated temperature differential scanning calorimetry (MT-DSC) with a DSCQ2000 from TA-instruments and was equal to 43.3 °C, 41.2 °C, 42.1 °C, and 43.2°C for EA-CC, EA-10P, EA20P, and EA-30P, respectively. Since the deviation of the measured T_g of the standard reproducible free film is 1.4 °C, the T_g's of these samples are considered similar. The similar T_g for samples with different PVCs and the clear coat as well as the absence of further residual activity and curing in MT-DSC measurements confirms that no modification has occurred in the curing of the samples due to the presence of pigments/extenders.

2.2. Electrochemical measurements

The ORP-EIS measurements were carried out in a conventional 3 electrode setup with a Pt mesh used as the counter electrode, and an Ag/AgCl (sat. KCl, $E^0 = 0.197$ V vs NHE) electrode as the reference electrode. A NI PCI-4461 data acquisition card connected to a custom-built compact analog potentiostat placed inside the Faraday cage was used for the data acquisition. This potentiostat is equipped with electrometer-grade input amplifiers. The signal used for ORP-EIS is a periodic

Table 1
Composition of the organic coatings as provided by the coating manufacturer, AkzoNobel. The quantity of the ingredients is reported in grams.

Application	Description	Clearcoat	PVC= 10%	PVC= 20%	PVC= 30%
	Component A				
Solvent	MIBK	76.1 g	71.8 g	67.0 g	61.6 g
Binder (epoxy resin) Equivalent weight	Medium solid liquid epoxy resin based on Bisphenol A 187 g/eq	51.8 g	48.9 g	45.6 g	42.0 g
Dispersing agent	Polymeric dispersant		0.6 g	1.2 g	1.9 g
Pigment	Titanium dioxide (Rutile) / TiO_2		10.1 g	21.3 g	33.7 g
Filler/ extender	Barium sulfate / $BaSO_4$		11.0 g	23.4 g	37.0 g
Filler/ extender	Talcum / $Mg_3Si_4O_{10}(OH)_2$		6.8 g	14.4 g	22.8 g
Flow additive	Polyacrylate solution	0.2 g	0.2 g	0.2 g	0.2 g
	Hardener				
	Component B				
Solvent	Xylene	38.1 g	35.9 g	33.5 g	30.8 g
Curing agent Equivalent weight	Cycloaliphatic amine 135 g/eq	37.4 g	35.3 g	32.9 g	30.3 g
	Thinner				
	Component C				
Solvent	4-methylpentan-2-one	7.9 g	7.5 g	22.3 g	44.6 g
Solvent	Xylene	4.0 g	3.7 g	11.2 g	22.3 g
	Exact PVC	0.0	10.0	20.1	30.2
	NV content vol%	30.3	30.3	30.9	30.3
	Epoxy/amine ratio	1.0	1.0	1.0	1.0
	Dry film density (g/ml)	1.12	1.39	1.66	1.93

broadband signal with randomly generated phases. In this signal, only odd harmonics of the base frequency are excited while one out of three consecutive harmonics is randomly omitted. The data acquisition is performed using a custom software operating under Python 3.7. The frequency range of the signal, amplitude and the number of periods were 5 mHz-1 kHz, 20 mV (rms), and 6, respectively. A 0.05 M NaCl solution was used as the electrolyte with a measurement surface area of 0.785 cm^2. The OCP of the samples was measured for 10 s and the measurements were started in less than 1 min after exposure of the samples to the electrolyte at room temperature.

ORP-EIS provides supplementary information on different noise levels contributing to the system's response such as stochastic noise, non-linearities and non-stationarities. In the measurements showing non-stationarities, the current response contributes to both excited and non-excited frequencies, forming so called "skirts" around the excited frequencies in the frequency domain. These skirts are modelled using Legendre polynomials and the results are deconvoluted in the time domain. In this way, the time-varying impedance (instantaneous impedance) is calculated. During the short immersion times (first 6 h) where the samples act non-stationary, instantaneous impedance is calculated and used for the electrochemical equivalent circuit (EEC) modelling. For the details on the calculation of instantaneous impedance, readers are referred to the work of Breugelmans et al. [34,35]. The statistical evaluations (one-way ANOVA test) were done using GraphPad Prism.

The fitting of the experimental data to the proposed mathematical models is performed through non-limiting fitting using the lmfit module in python 3.7.

2.3. Scanning electron microscopy (SEM) imaging

The microstructure of the coatings was observed on the cross-section by scanning electron microscopy (SEM) using a JEOL JSM-IT300 system. The back scattered electron detector (BSD) was employed with an acceleration voltage of 15.0 kV.

The cross-section of the samples was obtained by a cutting machine and the cut samples were mechanically ground with silicon-carbide papers down to 4000 grit and polished with a 1 μm diamond paste. Afterwards, the samples were ion milled using Hitachi ArBlade5000 cross-section polisher with 5.0 kV acceleration voltage of argon beam. Such a low value was chosen because of the polymeric content of the organic coatings.

2.4. Glow discharge optical emission spectroscopy (GDOES)

A glow discharge optical emission spectroscope (GDOES) with a GD Profiler 2 from HORIBA with a standard 4 mm diameter copper anode was used to obtain the elemental depth profiles. Argon gas plasma with an energy of ~50 eV, average pressure of 650 Pa and an applied power of 35 W were employed as source conditions for this analysis and each measurement was reproduced two times.

3. Results and discussion

3.1. Investigating the distribution of the pigments

The first insight into the morphology of the coatings and the distribution of pigments in the samples was obtained using scanning electron microscope (SEM) images of the cross-section. For EA-10P and EA-20P, a layered structure is visible consisting of a layer in the upper section of the coating where pigments are not present (non-pigmented layer), and a mixed layer in the bottom (pigmented layer). These two layers are displayed in Fig. 1.a. In EA-10P, the non-pigmented layer has an average thickness of 6.9 μm. In EA-20P, there is no clear line between the two layers, and the transition between the layers is not homogenous. Furthermore, with increase in pigmentation, at some spots marked with red circle in Fig. 1.b., the pigmented layer is extended towards the non-pigmented layer and the thickness of the non-pigmented layer is around 1 μm. In EA-30P, the coating structure is more homogeneous and only one pigmented layer is present with some areas only filled with the binder. The SEM images elucidate that for lower PVCs, sedimentation of the pigments has happened in the system. The change in the structure of the coatings with variations of PVC (bi-layer like structure), makes these samples interesting to investigate their electrochemical response in a corrosive media since different diffusion properties are to be expected. The SEM images (d-f) from the surface of the coatings also confirm the former results.

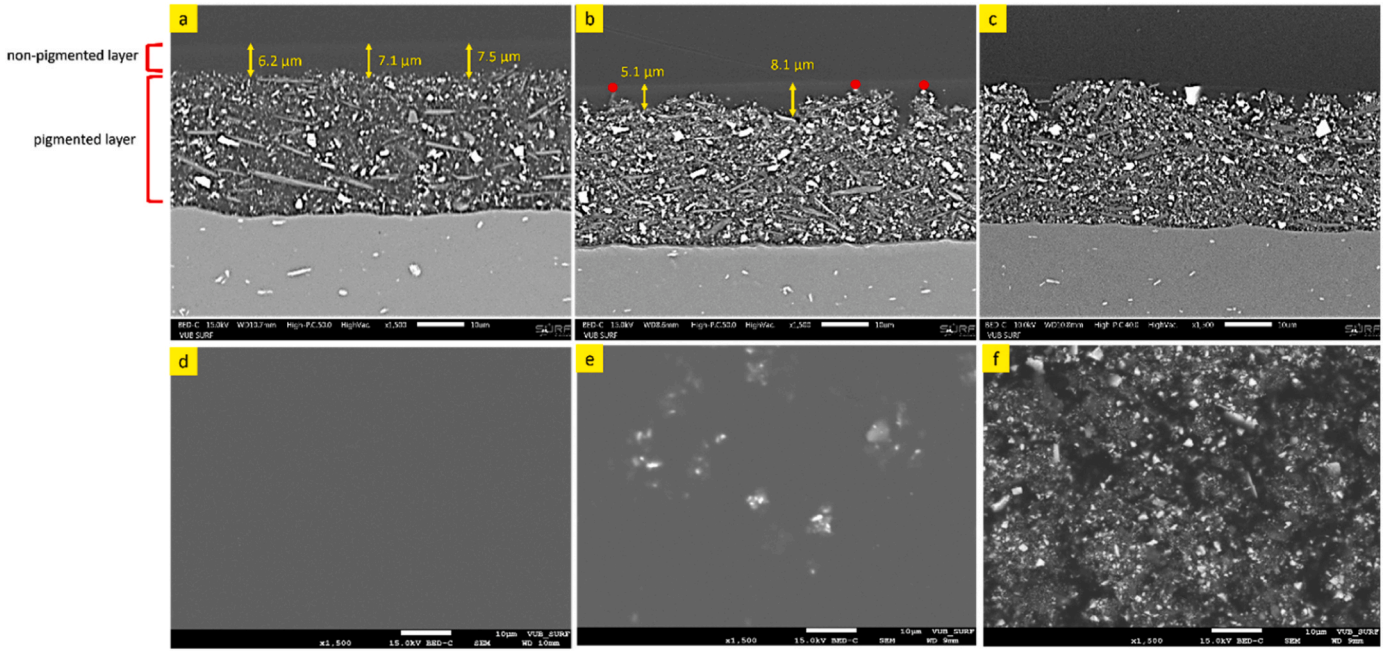

Fig. 1. Cross-section SEM images of the (a) EA-10P, (b) EA-20P and (c) EA-30P and the top view from the coating surface for (d) EA-10P, (e) EA-20P and (f) EA-30P.

3.2. Investigating the electrochemical response of the coatings

The Bode plots and Nyquist plots for the four samples exposed to 0.05 M NaCl electrolyte are shown in Fig. 2 and Fig. 3, respectively. To better understand the influence of pigmentation, ORP-EIS is also performed on the clearcoat (EA-CC). For EA-CC, the phase angle remains high and between − 80° and − 90° in almost the whole frequency range during the 111.82 (≈112) days of immersion. The impedance in the low frequency region is around 10 GΩ cm^2. The high value of the impedance at low frequency region, logarithmic decrease in impedance versus

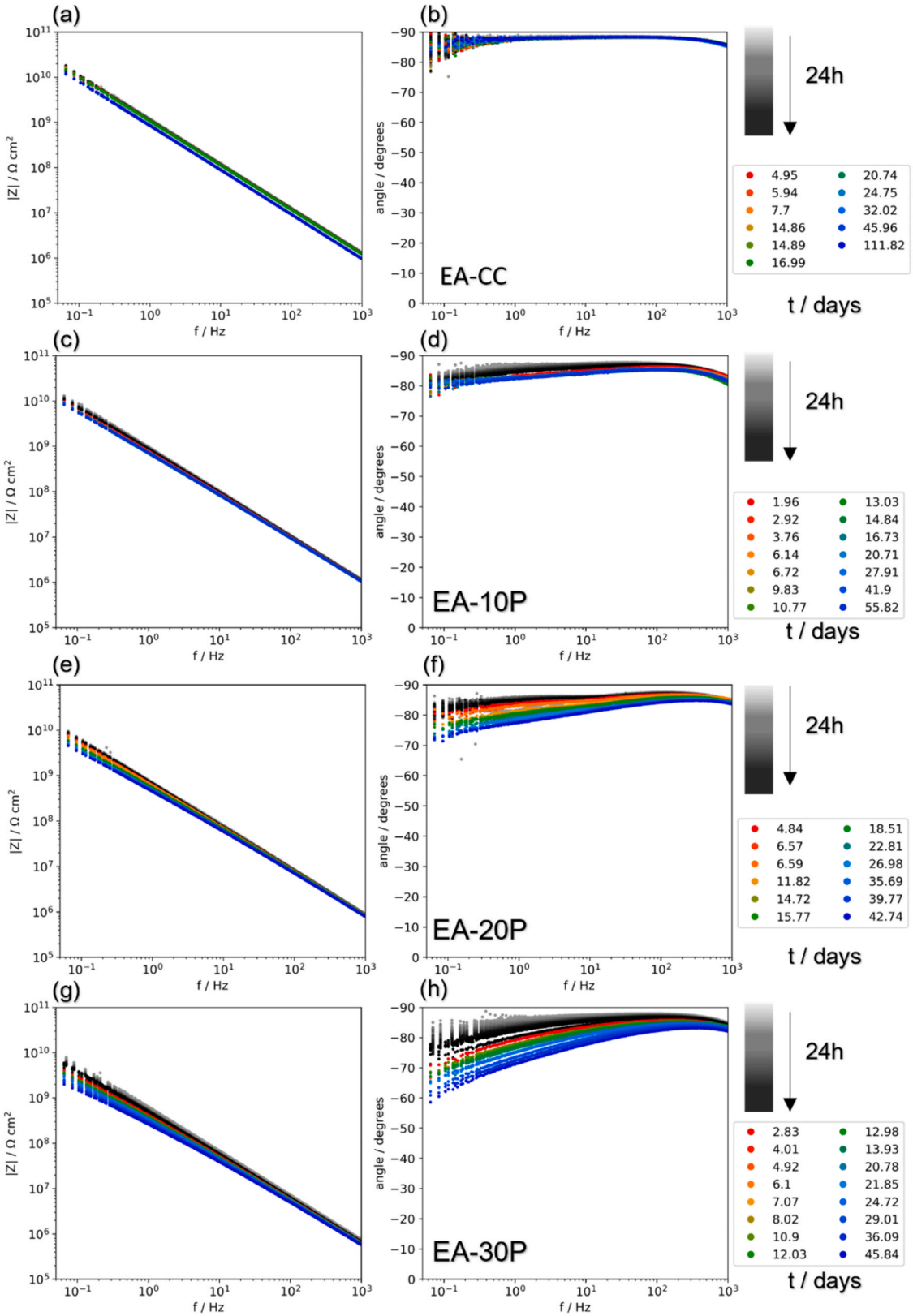

Fig. 2. Bode plots of: (a)&(b) EA-CC, (c)&(d) EA-10P, (e)&(f) EA-20P, and (g)&(h) EA-30P during different exposure times.

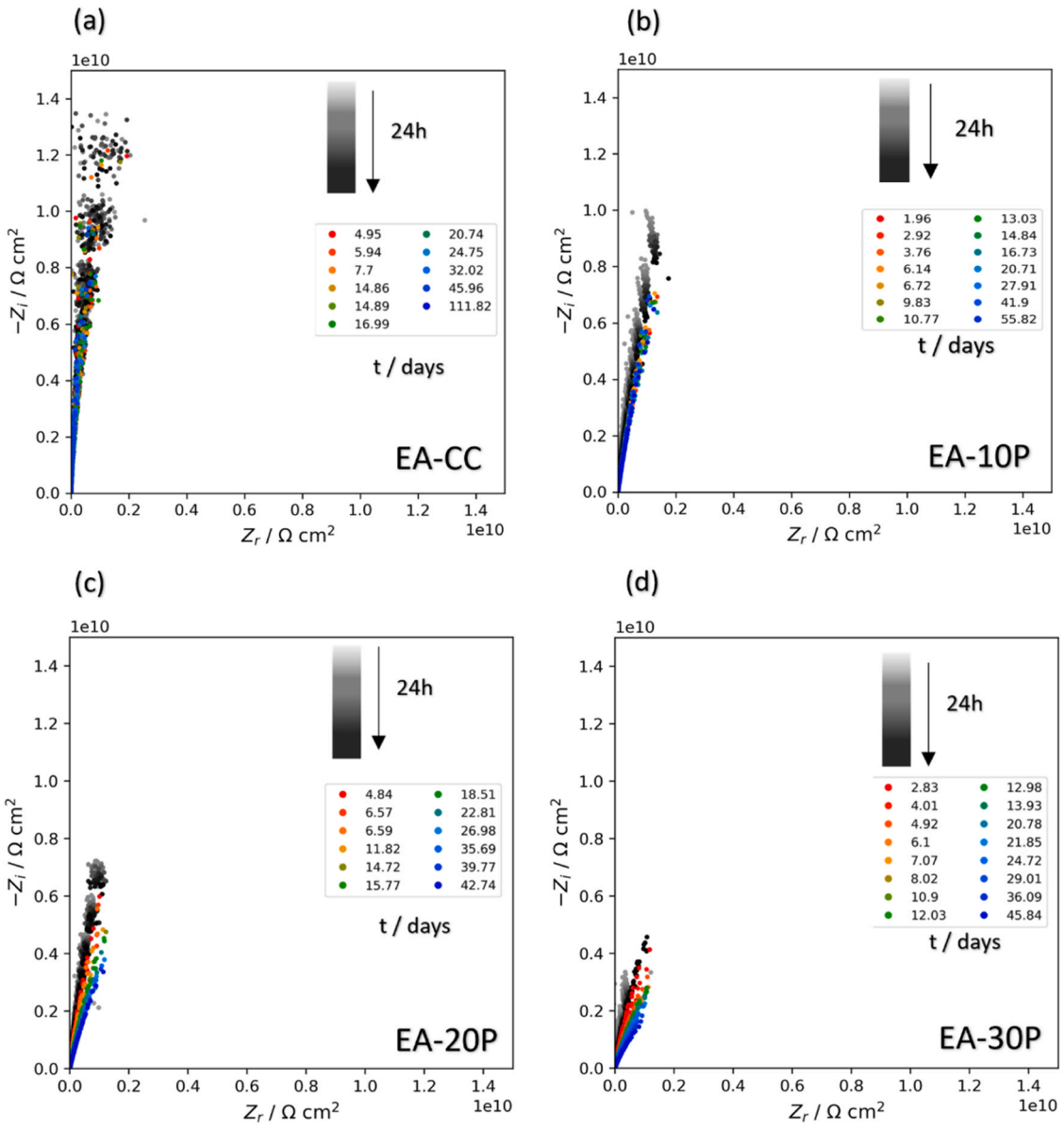

Fig. 3. Nyquist plots of: (a) EA-CC, (b) EA-10P, (c) EA-20P, and (d) EA-30P during different exposure times.

increasing frequency and high phase angle over the whole frequency range of the experiment, indicate high barrier properties of the EA-CC sample, even after long exposure times. However, small variations in impedance modulus and phase angle are visible.

For the EA-10P sample, similar to EA-CC, the impedance modulus in the low frequency region and the phase angle, maintain their high values during the immersion period. In EA-20P and EA-30P, the decrease in impedance in the low frequency region as well as the decrease in phase angle is more pronounced compared to the two former samples. On the other hand, EA-30P illustrates a faster decrease in impedance modulus in comparison with EA-20P with similar period of exposure to the electrolyte. The diminishing barrier properties of the coatings with increase in pigmentation is more obvious in the Nyquist plots shown in Fig. 3.

The ORP-EIS data of the four samples are modelled with the electrochemical equivalent circuit shown in Fig. 4, known as the two-layer model. This EEC has been used to model similar impedance plots in the literature [23,25,28,36–38]. The details of the data treatment procedure to verify the application of the two-layer model is explained in the work of Chen et al. and Wouters et al. [23,39]. The two-layer model is based on the presence of two layers in the coating, which are modelled in a series configuration towards the metal oxide/coating interface. These two layers have different resistivity profiles which can originate from different phenomena. Concerning organic coated metals exposed to an aqueous electrolyte, one of the possible origins of this dual behaviour is found to be the delayed diffusion of ions with respect to the water. The outer layer of the coating poses an exponential resistivity distribution in presence of ions, while the inner layer has a different resistivity profile because of the absence of ions. In presence of the exponential resistivity distribution, a Young impedance can model the behaviour of the sample [40]. Madelat et al. have used this model to deconvolute and analyse the separate diffusion of ions in polyethylene glycol diacrylate (PEGDA) coatings with thicknesses equal to 100 and 150 μm [25]. On the other hand, they have shown that with the increase in thickness of the coating to 200 μm, the two-layer EEC cannot follow the diffusion of ions further and rather models the two compositionally/structurally distinct layers of the coating. Hence, this EEC is interesting to investigate these pigmented epoxy-amine coatings, since the resistivity distribution in these coatings can have two different origins: diffusion of ions and layers with different structure/morphology.

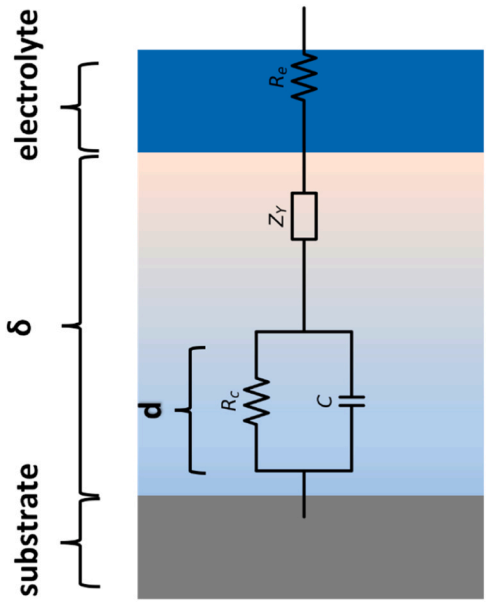

Fig. 4. Schematic description of the two-layer model. **δ**, thickness of the coating; **d**, thickness of the inner layer, $\mathbf{R_c}$ resistance of the inner layer of the coating; **C**, capacitance of the inner layer of the coating; $\mathbf{Z_Y}$, Young impedance for the outer layer of the coating; $\mathbf{R_e}$, electrolyte resistance.

To evaluate the goodness of fit, the noise+non-stationarities levels are used as a statistical tool. As mentioned in the experimental section, only odd harmonics of the base frequency are excited in ORP-EIS and one out of three consecutive harmonics is randomly omitted. In this way, different noise levels can be calculated from the standard deviation of the response recorded over excited and non-excited frequencies, i.e., stochastic noise, non-stationarities and non-linearities. Since non-stationarities are the standard deviation over excited frequencies, they show the variation of the actual data. Therefore, if the residual of the model is at the same order of magnitude as the noise + non-stationarities, the error of the model is not exceeding the variation of the data, verifying a good yield between the fit and the experimental data [21,31,32,35]. With increase in immersion time, the system becomes stationary and the model residual does not overlap with noise+non-stationarities over the whole frequency domain. There, the model can be considered accurate as long as the relative residual remains below 10%.

3.2.1. *Investigating the electrochemical response of the clearcoat (EA-CC)*

The ORP-EIS data are fitted to Eq. 1 [41–43] to extract the time evolution of the output parameters. The parameters evolution is illustrated in Fig. 5 for EA-CC. With reference to the schematic of the two-layer model in Fig. 4, $\boldsymbol{d}$ is the thickness of the inner layer. If the difference in the two layers is assumed to be due to the presence of ions, the inner layer would be the ion free zone of the coating and the time evolution of $\boldsymbol{d}$ would represent the ingress front position of the ions. In this case, with arrival of the ions at the metal oxide/coating interface, $\boldsymbol{d}$ approaches to zero. The maximum value of $\boldsymbol{d}$ can be equal to the thickness of the coating ($\boldsymbol{\delta}$). $\boldsymbol{\varepsilon}$ is the dielectric constant of the coating. $\boldsymbol{\varepsilon}$ for organic coatings is mostly reported between 3 and 8 [44]. However, $\boldsymbol{\varepsilon}$ changes by ingress of the electrolyte, considering the high value of the dielectric constant of water (78.4 at 25°C). The increase in $\boldsymbol{\varepsilon}$ is often correlated to the uptake of water [45,46]. The exponential resistivity distribution in the outer section of the coating can be explained using Eq. 2 [40,47]. With reference to this equation, λ or the characteristic length, is indicative of the sharpness of the resistivity profile. In general, with further penetration of the ions in the coating, the resistivity gradient over the thickness decreases, which corresponds to an increasing evolution of λ. $\boldsymbol{\rho_c}$ on the other hand, is the resistivity of the coating. Eventually, $\boldsymbol{R_e}$ corresponds to the resistance of the electrolyte.

$$Z = d\frac{\rho_c}{1 + j\omega\varepsilon\varepsilon_0\rho_c} - \frac{\lambda}{j\omega\varepsilon\varepsilon_0}\ln\left(\frac{1 + j\omega\varepsilon\varepsilon_0\rho_c\exp\left(-\frac{\delta-d}{\lambda}\right)}{1 + j\omega\varepsilon\varepsilon_0\rho_c}\right) + R_e \quad (1)$$

$$\rho(x) = \rho_c\exp\left(-\frac{x}{\lambda}\right) \quad (2)$$

With reference to Fig. 5.a. for EA-CC, the evolution of $\boldsymbol{d}$ starts around 25.5 μm and doesn't go below 23 μm during the entire immersion time. The measured thickness of the coating is 30 ± 3 μm using scanning electron microscopy (SEM) images. To fit the data with the two-layer model, the thickness of the coatings is assumed constant and equal to 30 μm. About the value of $\boldsymbol{d}$ not starting from 30 μm it should be considered that at each time spot, $\boldsymbol{d}$ shows where the ingress front of the ions is positioned and the time between pouring the electrolyte in the corrosion cell, closing the Faraday cage and 10 s of the OCP measurement, gives some time to the ions to penetrate deeper before starting the measurement. Based on the evolution of $\boldsymbol{d}$, the penetration depth of ions is around 7 μm after 112 days of immersion in electrolyte. $\boldsymbol{\varepsilon}$ has an increasing trend during the first 48 h and stays constant for almost 650 h. Hereafter, a sudden increase leading to the second plateau is reproduced in 3 samples. This sharp increase may be an indication of the swelling and/or interfacial dynamics such as delamination and accumulation of water. Further investigations are thus required to identify the origin of this sudden increase. λ and $\boldsymbol{\rho_c}$ values are fluctuating around 0.5 and 1e12 Ω m, respectively. However, a general increasing trend can be seen for λ. The increase in λ indicates further diffusion of ions. Prior to the sharp increase in $\boldsymbol{\varepsilon}$, $\boldsymbol{R_e}$ is also stable and its changes can be considered negligible.

GDOES measurements are performed on the reference EA-CC sample not exposed to the electrolyte (EA-CC-Ref) and on the sample exposed to the 0.05 M NaCl electrolyte for 120 days (EA-CC-120d) to gain insights about the distribution of the penetrating species and validate the profile obtained for $\boldsymbol{d}$. Based on the composition of the coatings, depth profiles are obtained for C, O, N, and Al. The depth profiles of Na and Cl in the reference and sample exposed for 120 days is presented as well. As shown in Figs. 6, 3 zones are determined. Zone I is where the C and O intensities are decreasing. It takes 100 s for the intensity of these elements to reach a plateau. For N, there is no clear trend of changes obvious, and its intensity is stable all along the thickness. The average thickness of this sample is 30 μm. Considering that 930 s of sputtering should approximately correspond to 30 μm, the thickness of zone I is around 3.2 μm. In zone II, all the elements demonstrate constant intensity. Zone III is considered as the region where the intensity of Al (from the substrate) starts to rise. Based on GDOES results, the composition of the coating in the upper part (thickness ≈3.2 μm) is different. Indeed, the intensity of C and O is higher while the intensity of N is stable all over the thickness. In the samples exposed to the electrolyte for 120 days, the intensity of Na and Cl has increased in comparison with the reference. However, the depth of penetration of Cl is more than Na. For Cl, the depth of penetration is approximately around 8 μm (250 s of sputtering). The depth of penetration of ions was calculated from ORP-EIS measurements to be around 7 μm. As such, this value corresponds well to the depth profiles of the exposed sample where the depth of penetration of Cl is approximately around 8 μm. The enhanced diffusion of ions in the upper section of the coating can be correlated to its distinct chemistry. Since GDOES confirms the output of ORP-EIS, the compositionally different layer on the top does not impose a dominating influence on the resistivity distribution profile and hence two-layer EEC can follow the diffusion of ions. Concerning the deeper penetration of chlorides, it has been discussed in the literature that Cl^- has a smaller hydration cell compared to Na^+, which can result in their faster diffusion [48,49].

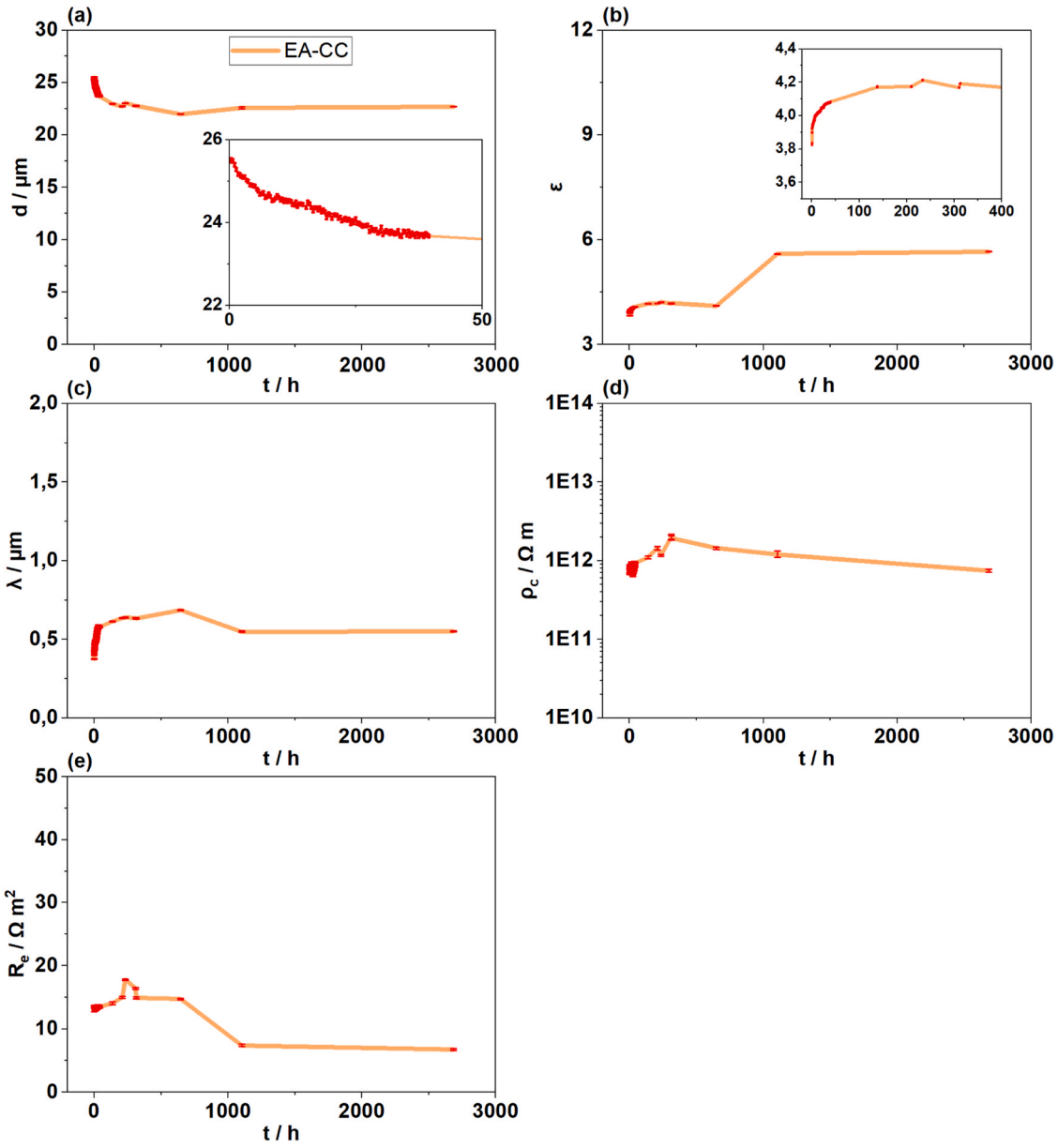

Fig. 5. Output parameters of the fitting of the EA-CC ORP-EIS data to Eq. 1: (a) Thickness of the inner layer **d**, (b) dielectric constant **ε**, (c) characteristic length **λ**, (d) coating resistivity ρ_c, and (e) electrolyte resistance R_e. The parameter errors are shown as errorbars on each datapoint.

3.2.2. Investigating the electrochemical response of the pigmented coatings

For EA-10P, as shown in Fig. 7, ***d*** starts from 22 µm and decreases to 11 µm after 90 h, staying approximately constant during the remaining immersion time. Therefore, based on the results shown in this figure, the inner layer does not disappear during exposure time. The value of ε is initially equal to 4.69. With further diffusion of water, it increases to $\varepsilon \approx 5.27$ and stays constant with negligible fluctuations. The constant value of ε can be an indication of saturation of the coating with water. λ has an increasing trend, showing that the resistivity profile becomes more uniform. This value is stable after about 90 h. ρ_c has an initial decreasing trend and stabilizes around 1e12 Ωm. The behaviour and the value of the parameter ρ_c is similar between EA-CC and EA-10P.

GDOES results for EA-10P are displayed in Fig. 8 for the reference sample not exposed to the electrolyte (EA-10P-Ref) and the sample exposed to the electrolyte for 120 days (EA-10P-120d). In this figure, 4 zones are determined. In zone I, the intensity of O and C have a decreasing trend and the elements related to the pigments (Ba, Ti, Mg, Si) have their minimum intensity. Similar to EA-CC, the intensity of N is constant in zone I. In zone II, all the elements except Al show an abrupt increase in their intensities. In zone III, the intensity of the elements either is constant or shows a slight increase. Zone IV identifies the substrate by the increase in the intensity of Al. The border of each zone is determined approximately. As such, in EA-10P-Ref sample it takes 520 s of sputtering to reach the interface (zone IV) while for EA-10P-120d, it takes 570 s of sputtering to approach the Al substrate. The difference in the sputtering time to reach the buried interface in these two samples is due to the difference in the thickness of the applied coating. To avoid complexity only the line corresponding to 520 s for EA-10P-Ref is shown on this figure.

These data unravel the layered structure of the coating and zone II can be considered as a transition zone between the two layers with different compositions. Based on the GDOES results, EA-10P has an outer layer where pigments are absent and the sputtering of this outer layer takes about 200 s. Considering that the sputtering rate in presence and absence of inorganics significantly differs, the sputtering rate of EA-CC can be used to calculate the thickness of this outer layer which results

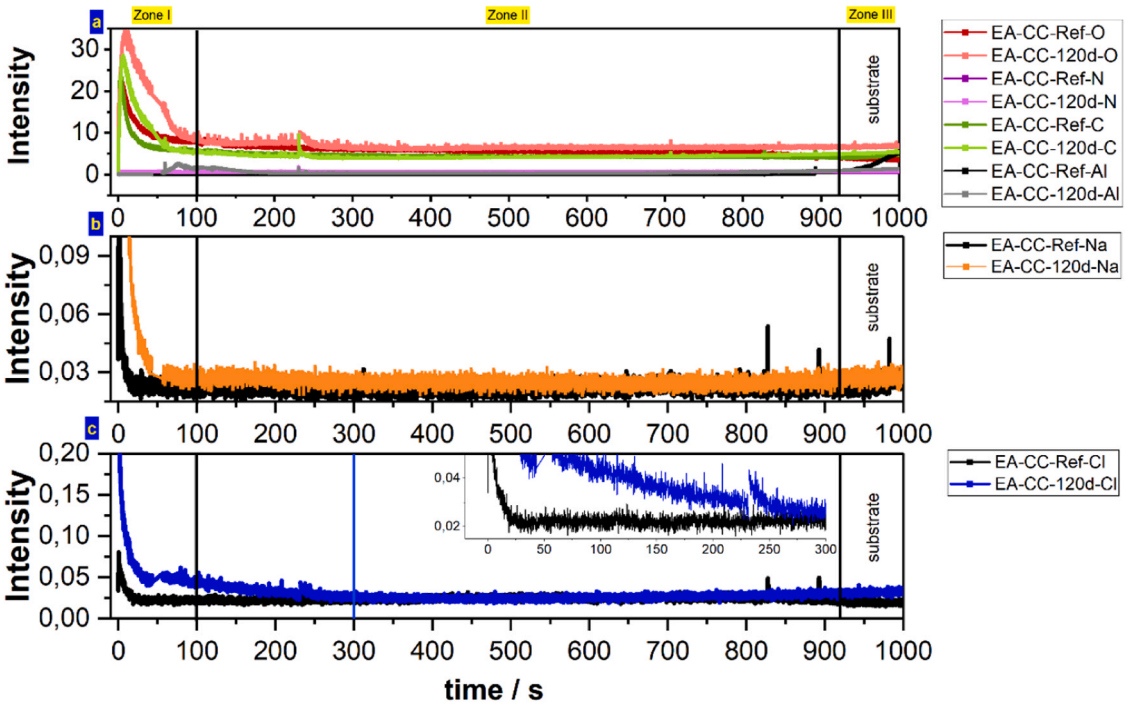

Fig. 6. GDOES elemental depth profiles of EA-CC sample: (a) depth profile of O, N, C and Al; (b) depth profile of Na; (c) depth profile of Cl for the reference sample and the sample exposed for 120 days.

in a value of around 6.4 μm. This value corresponds well to the SEM images where the thickness of the non-pigmented zone was reported to be 6.9 μm. For the transition zone, the sputtering rate of the EA-30P sample is used, since in that sample inorganic pigments are present all over the thickness as displayed in SEM images, Fig. 1. In EA-30P, approximately 400 s of sputtering is associated with 30 μm. Using this sputtering rate, zone II in EA-10P samples has a thickness close to 8.2 μm.

Fig. 8.c. and Fig. 8.d. display the depth profiles of Na and Cl. It's clear that the intensity of these ions penetrating from the surrounding electrolyte is higher in the exposed sample in zone I. In zone II and zone III, the intensity of Na and Cl follow the same evolution as the other elements. The increase in the intensity of Na and Cl in zone II and III should be further investigated since this increase occurs simultaneously with increase in the amount of the pigments present in these zones, indicating that these ions are most likely incorporated in the pigments' composition. The increase in the concentration of these ions in zone II and III makes it difficult to calculate the depth of the penetration of the ions, as the intensity of the ions present in zone II and III is higher than the intensity of the diffusing ions from the surrounding electrolyte. However, the depth profile of Na in the exposed sample overlaps with its depth profile prior to exposure in the reference sample, after 100 s of sputtering. From this graph, the depth of penetration of Na is calculated around 3.2 μm with respect to the sputtering rate of EA-CC. Absence of a well-defined baseline in the depth profile of Cl due to the increasing trend of the intensity, prevents us from estimating the penetration depth of chloride ions. GDOES results for EA-CC showed that the depth of penetration of Na and Cl are not equal, and chlorides can proceed faster and deeper. Hence, the depth of penetration of Cl in these coatings cannot be simply considered as equal to Na and might be deeper.

ORP-EIS results show that the thickness of outer layer does not go above 19 μm during the whole immersion time. This value roughly corresponds to the thickness of the outer layer plus the thickness of the transition layer (6.4 +8.2 =14.6 μm). This correspondence indicates that the two-layer model follows the diffusion of ions till their arrival at a certain depth after which the resistivity distribution is dominated by the change in the morphology/structure. From this point, the two-layer EEC models the two compositionally different layers in the coating instead of modelling two compositionally identical layers whose only difference is the presence and absence of penetrating ions. It should be mentioned that the composition between two layers changes gradually as shown by the presence of a transition zone. Therefore, it can be concluded that the resistivity distribution arising from the change in the composition of the coating imposes a limiting condition to the EEC modelling and the interpretation of the results should be done carefully. Hence, stabilization of d at values around 11 μm in EA-10P EEC fitting results actually show the transition to the second layer of the coating instead of showing the penetration depth of ions.

Similar to EA-10P, d starts around the value of 20–22 μm for the other two pigmented coatings. For the EA-20P sample, the inner layer fades out between 954.37 and 1025.75 h (39.77–42.74 days) and for EA-30P, the inner layer disappears between 524.4 and 593.34 h (21.85–24.72 days) after immersion as shown in Fig. 7. After this time, the two-layer model is not able to explain the behaviour of the samples further. Hereafter, a modification of the model is required to include the physical representation of the changes in the electrochemical response of the system. Madelat et al. have shown that with arrival of the ions at the buried interface, the changes in the electrochemical state of the system can be due to the interfacial influences [28]. The initial value of ε is different for each sample. Addition of the pigments is increasing the measured dielectric constant, as EA-30P has the highest dielectric constant. The ε of the components of the coating can affect the measured ε, e.g., ε of TiO_2 is higher than the one of the organic coating and with increase in concentration of the pigments, the measured ε will also increase [50]. For EA-20P and EA-30P, ε has an increasing trend during the measurement. λ has an increasing behaviour in EA-20P and EA-30P, while having higher values in the latter. Higher values of λ mean that the concentration gradient of ions in the outer layer is smaller, resulting in a more uniform resistivity profile. Therefore, with reference to this parameter, the concentration of ions penetrating to the EA-30P should be higher than all the other samples. On the other hand, the trend of the changes in ρ_c is also similar among all 4 samples while EA-30 has the lowest value. ρ_c as the resistivity of the coating is influenced by different factors such as the coating composition and the water uptake. R_e is

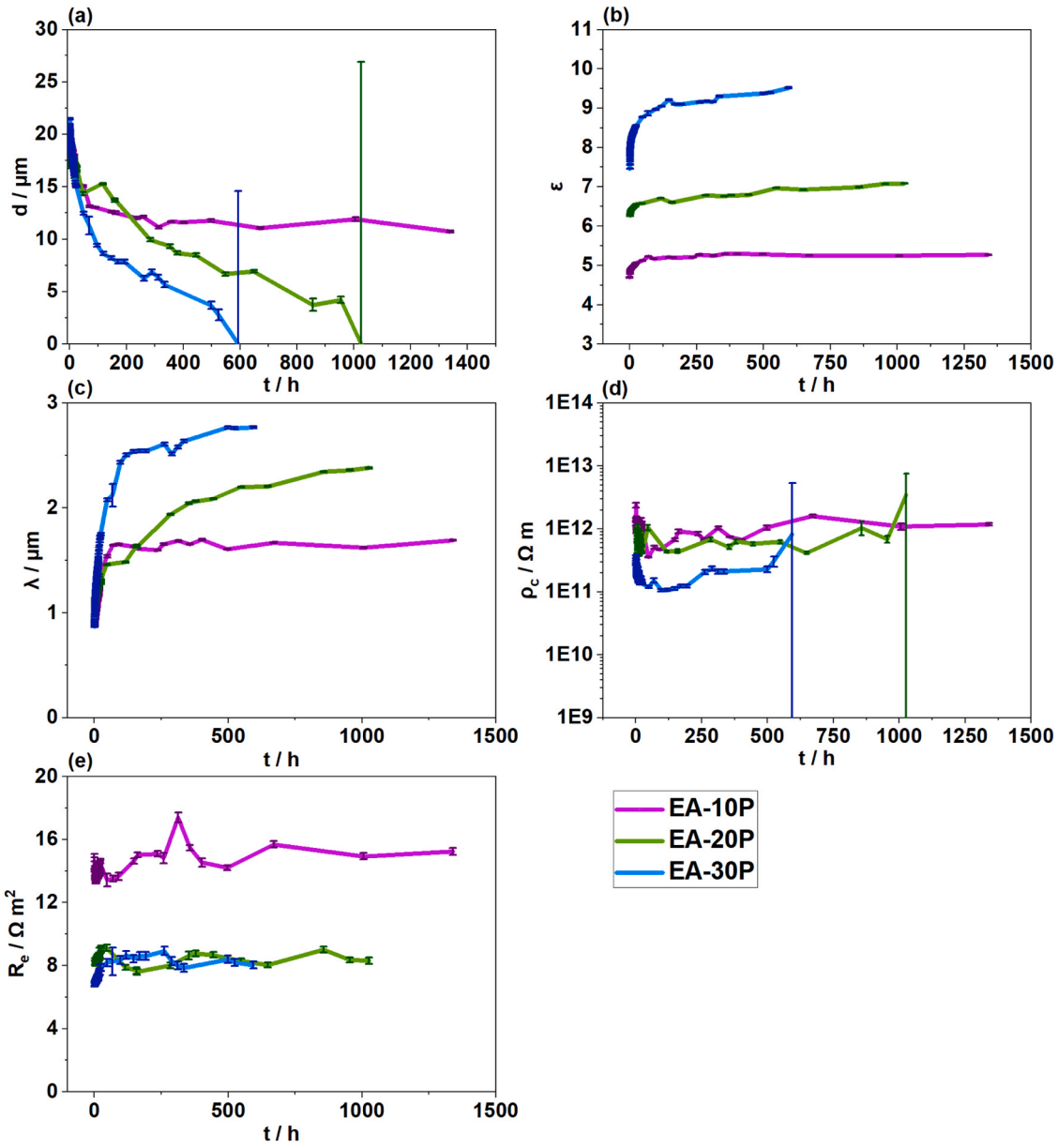

Fig. 7. Output parameters of the fitting of the EA-10P (purple), EA-20P (green), and EA-30P (blue) ORP-EIS data using Eq. 1: (a) Thickness of the inner layer **d**, (b) dielectric constant ε, (c) characteristic length **λ**, (d) coating resistivity $\boldsymbol{\rho_c}$, and (e) electrolyte resistance $\mathbf{R_e}$. The parameter errors are shown as errorbars on each datapoint.

constant for all samples.

Fig. 9 presents the GDOES depth profiles for the EA-20P reference sample (EA-20P-Ref), the sample exposed for 40 days (EA-20P-40d) and the sample exposed for 120 days (EA-20P-120d). The sample exposed for 40 days is measured as well since the arrival time of ions at the buried interface is determined around 40 days in ORP-EIS measurements. Similar to EA-10P, the whole spectrum is divided in 4 zones. In zone I, the intensity of O and C are decreasing. In zone II (transition zone), the intensity of all the elements (except Al) has an increasing trend. In zone III, almost all elements have constant intensities. The sputtering time required to reach the buried interface varies in different samples due to the difference in their thicknesses. Hence, EA-20P also has a heterogenous layered structure while the thickness of zone I (the non-pigmented layer) is smaller in EA-20P in comparison to EA-10P. Here, this layer is being sputtered away after 25 s, which is less than 1 µm. This value also corresponds to the SEM images.

For Na and Cl, the exposed samples have higher intensities in zone I and the initial part of the zone II. The intensity of Na is higher in EA-20P-120d in zone I and in half of the thickness in zone II than in the other two samples. There is no difference in the intensity of Cl in EA-20P-40d and EA-20P-120d. In the Cl depth profile, a peak appears in zone II. The origin of this peak remains under study. Calculation of the exact depth of penetration for ions is difficult due to the appearance of the peak in the Cl profile and sudden increase in the intensity of Na in zone II with increase in the concentration of the pigments. The change in the sputtering rate in zone I and zone II also increase the complexity of the calculation. In EA-20P, despite the layered structure of the coating, the resistivity distribution originating from the ion diffusion is still dominating the resistivity distribution arising from the layered structure of the coating. Therefore, the two-layer model is still capable of following the ion diffusion and can monitor their arrival at the buried interface. The dominating influence of the ion diffusion over the resistivity profile is most likely due to higher concentration of the ions penetrating the coating, which can be confirmed by comparing the intensity of these

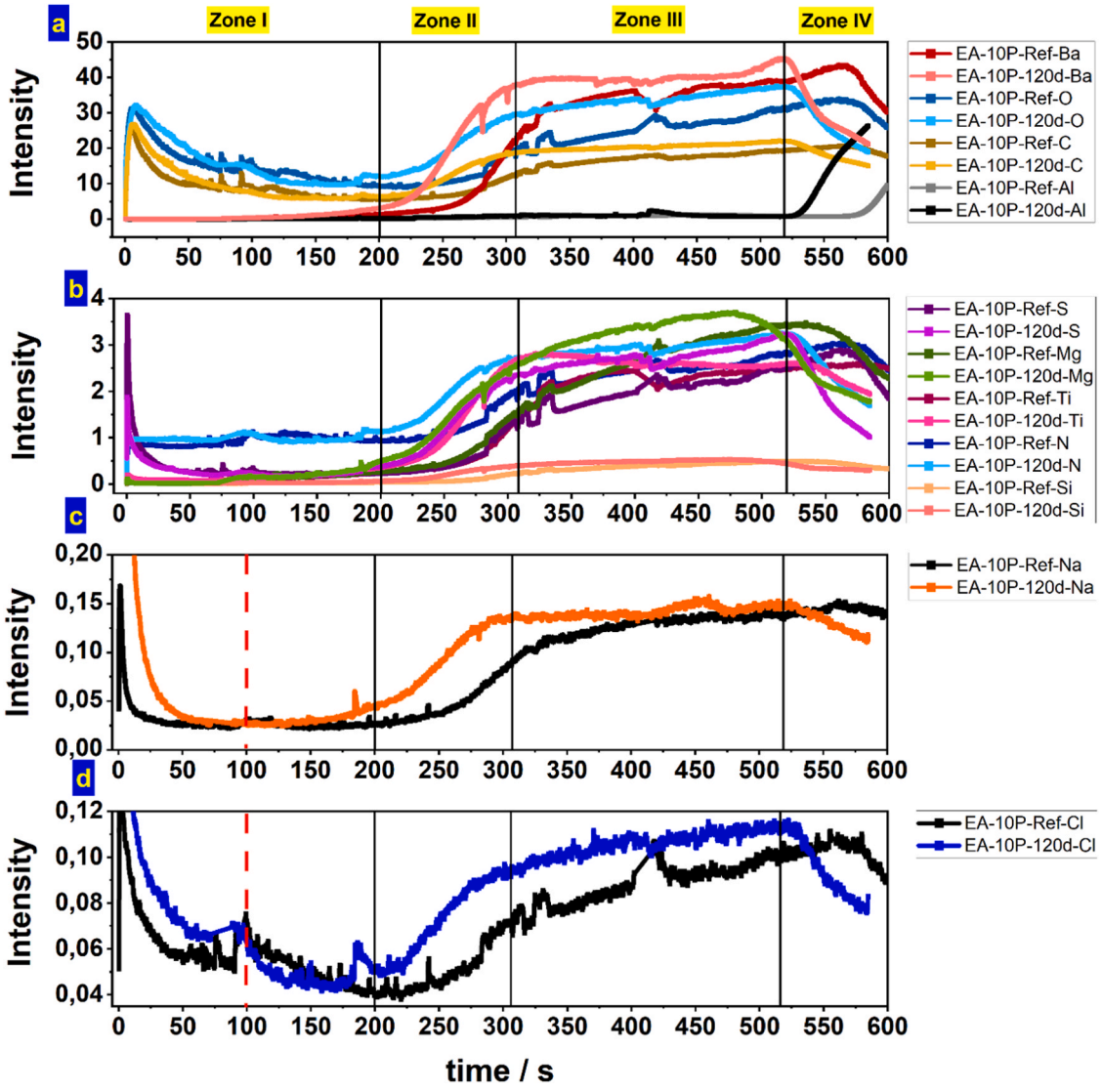

Fig. 8. GDOES elemental depth profiles for EA-10P: (a) depth profile of Ba, O, C and Al; (b) depth profile of S, Mg, Ti, N and Si; (c) depth profile of Na; (c) depth profile of Cl; for the reference sample, and the sample exposed for 120 days.

ions in EA-10P and EA-20P in Fig. 8 and Fig. 9.

For the EA-30P sample (Fig. 10), the zone I is the transition zone itself and no non-pigmented layer could be detected. Therefore, the depth of penetration of ions can be measured more accurately. For the sample exposed for 40 days (EA-30P-40d) and for the one exposed for 120 days (EA-30P-120d), chlorides are detected at the coating/metal oxide buried interface. For Na, no ions are detected at the buried interface in EA-30P-40d, while they have arrived at the interface in EA-30P-120d. Based on GDOES depth profiles, the concentration of ions penetrating EA-30P is higher than for other samples, as in the following sequence: EA-30P > EA-20P > EA-10P > EA-CC. Therefore, it can be concluded that ORP-EIS and GDOES correspond well with each other on EA-30P.

3.3. Water uptake calculation

Water uptake of the samples is calculated from the EEC modelling output of the ORP-EIS data (the evolution of the dielectric constant) using the well-known linear relationship (Eq. 3) and the results are illustrated in Fig. 11 [38,46,51]. For the initial 6 h after immersion, instantaneous impedance data is used respecting the enhanced non-stationarities. The dielectric constant of the coatings in the ''dry conditions'', ε_c, for each sample is estimated through the linear regression of ε versus $\sqrt{t}$ plots using bootstrap method with 10,000 iterations [52]. ε_c is estimated equal to 3.9 ± 0.05, 4.43 ± 0.11, 6.47 ± 0.03, and 6.99 ± 0.03 for EA-CC, EA-10P, EA-20P, and EA-30P, respectively. As mentioned before, the difference in ε_c is most likely coming from the change in the composition of the coatings and presence of pigments. It's noteworthy that in the linear mixture approach, the water distribution is assumed uniform and the influence of swelling is neglected. Therefore, the values obtained from this equation are an estimation of the real water uptake. In Eq. 3, ε is the dielectric constant of the coating in "wet conditions" at each corresponding time spot, ε_c is the dielectric constant of the dry coating, and ε_w is the dielectric constant of water. $\varnothing_w, V$ is thus the volumetric water uptake.

$$\varnothing_w, V = \frac{\varepsilon - \varepsilon_c}{\varepsilon_w - \varepsilon_c} \tag{3}$$

With reference to Fig. 11, all the coatings follow a pseudo-Fickian behaviour where a fast Fickian diffusion is followed by a slower diffusion. Unlike the EA-10P, a plateau region is not detected in EA-20P and EA-30P during the period of the measurement. On the other hand, the value of water uptake in EA-10P and EA-20P approach each other at

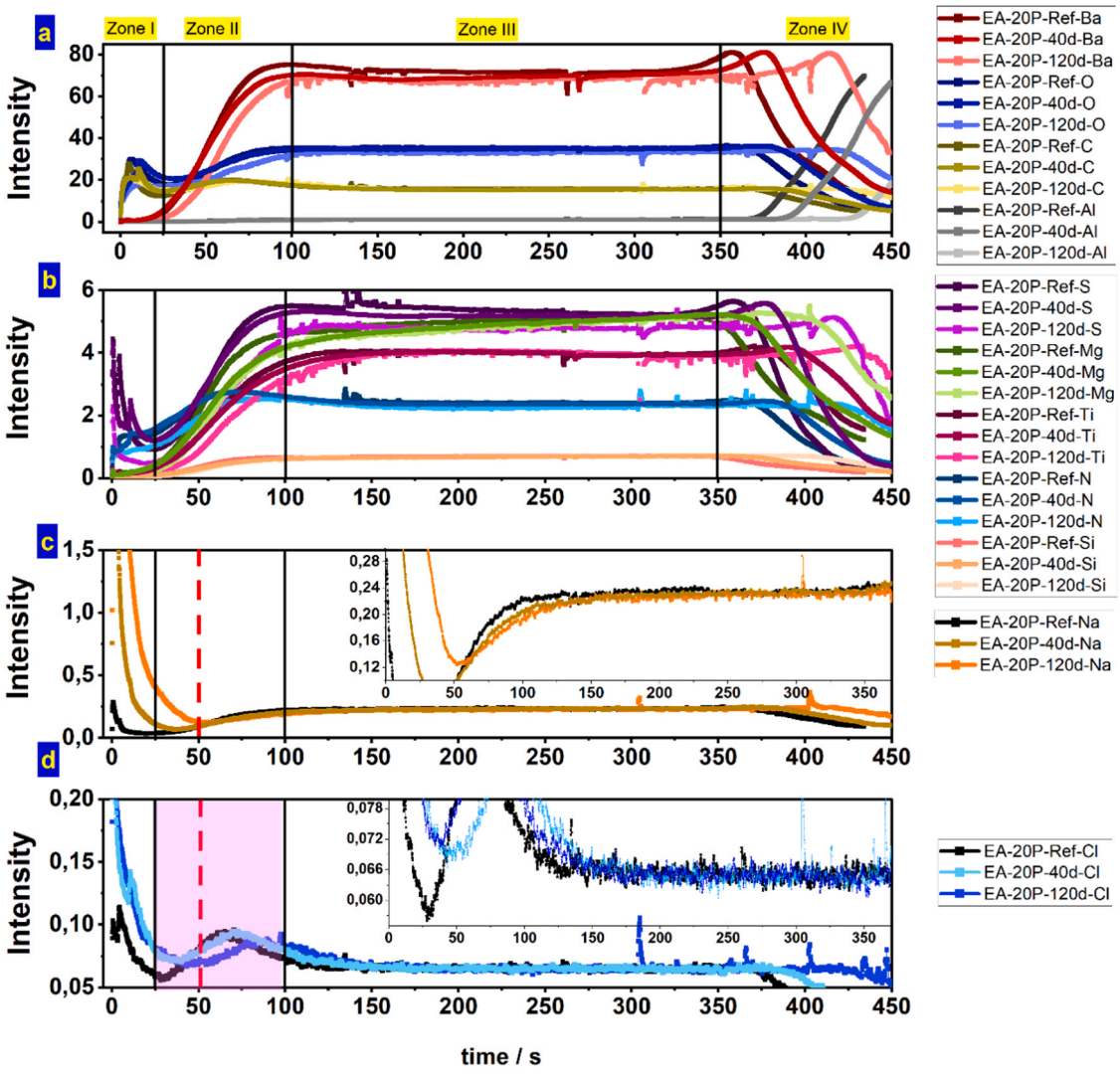

Fig. 9. GDOES elemental depth profiles for EA-20P: (a) depth profile of Ba, O, C and Al; (b) depth profile of S, Mg, Ti, N and Si; (c) depth profile of Na; (c) depth profile of Cl; for the reference sample, the sample exposed for 40 days, and the sample exposed for 120 days.

longer exposure times. The water take-up profile of EA-CC hits a plateau in longer exposure times and after 27 days, a sharp increase appears in the plot. The origin of this sharp increase is still under study.

The initial Fickian behaviour is mainly restricted to the first 2 h (ε follows a linear relationship with respect to $\sqrt{t}$ during this period) in all the samples and could be modelled using Eq. 4 to extract the initial diffusion coefficient [23,53]. The comparison of D among different samples is shown in Fig. 12. A one-way ANOVA test demonstrates that the slight decreasing trend evidenced is not significant and the variation between the initial diffusion coefficients of different coatings is negligible (one-way ANOVA; $P > 0.05$).

From the absence of the plateau region in EA-20P and EA-30P and the highest value of $\varnothing_w, V$ for EA-30P, it can be deduced that with the increase in the loading of pigments, water uptake is promoted. The pigment/binder interface could possibly provide more areas capable of hosting water, increasing the final concentration of water present in the system. This higher water uptake in EA-20P and EA-30P can also be due to the components of the coating leaving the matrix, e.g., entrapped solvents, generating cavities for the further penetration of water. In addition, the change at the coating/metal oxide buried interface triggered with the change in the composition of the coating and stress built-up should not be neglected. All these parameters may play a role in the enhanced water uptake of the systems with higher pigmentation.

$$\frac{\varnothing_w, V \quad (t)}{\varnothing_s} = 1 - \frac{8}{\pi^2}\exp\left(\frac{-\pi^2 Dt}{4\delta^2}\right) - \frac{8}{9\pi^2}\exp\left(\frac{-9\pi^2 Dt}{4\delta^2}\right) \tag{4}$$

The pseudo-Fickian diffusion of water in glassy polymers has been postulated to arise from the structural heterogeneities and/or structural relaxations of the polymer [4,54]. Similar to this work, Lacombre et al. reported a pseudo-Fickian diffusion process in an epoxy-based model coating. They correlated this behaviour to the decrease in the available polar groups interactions with diffusing water molecules at longer immersion times resulting in a time dependant diffusion coefficient [9,10]. Concerning the evolution of D, an initial stationary regime is followed by a transient regime where the diffusion coefficient D decreases significantly. The third step is the stabilization of D at its minimum value. Furthermore, Roggero et al. have shown that in a polyepoxy varnish below T_g, a pseudo-Fickian water uptake occurs which is due to the distribution of diffusion process such as the distribution of diffusion coefficients in a partially plasticized sample [55].

Lacombre et al. have also investigated the influence of TiO_2 pigments (with maximum level of 20 wt%, PVC=7%) on the diffusion of water and similar values of D were identified for the clearcoat and the pigmented coating at 30 °C during the first stage, which is in line with the similar initial diffusion coefficient observed for the coatings under the study. However, the difference of D between the clearcoat and

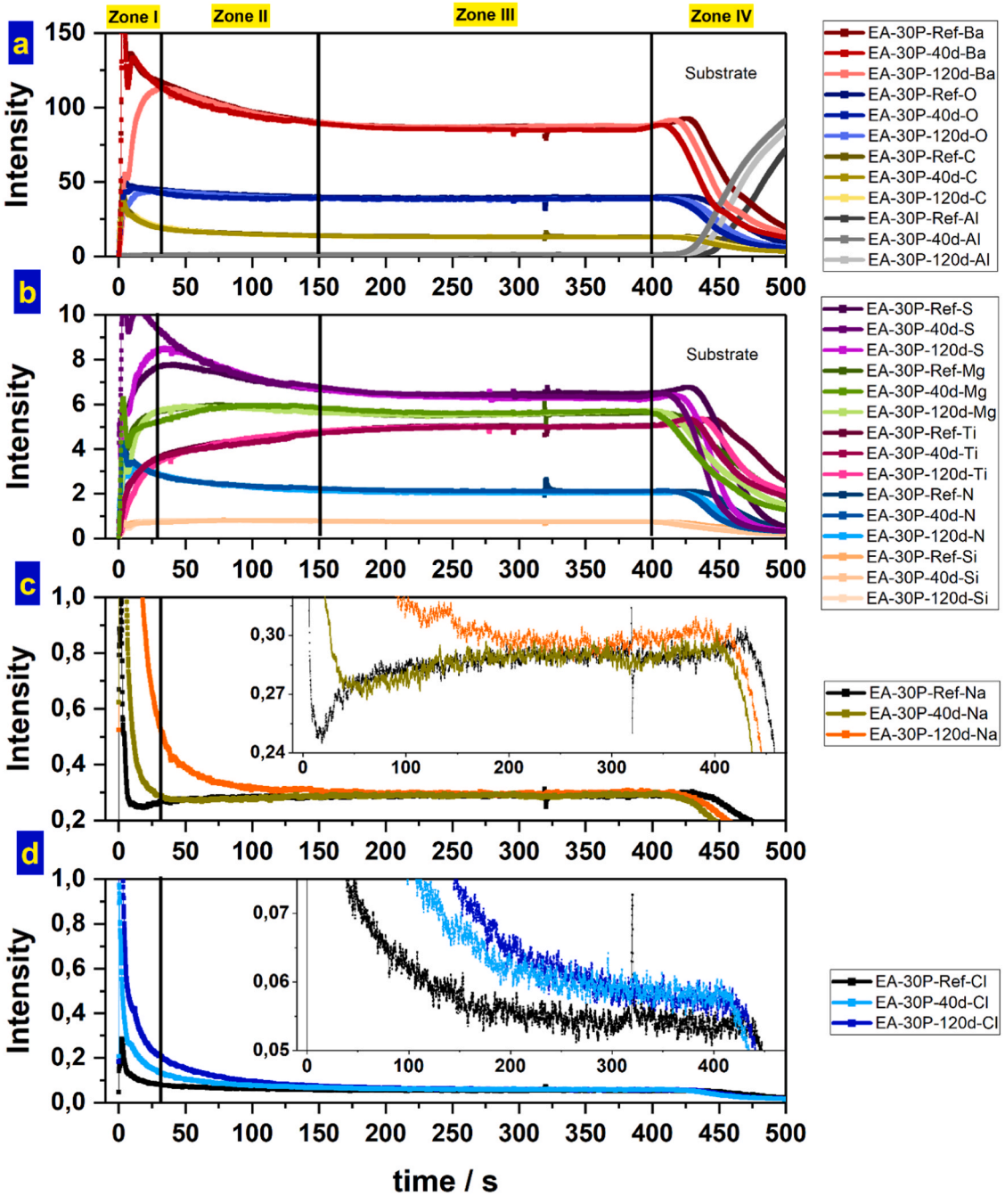

Fig. 10. GDOES elemental depth profiles for EA-30P: (a) depth profile of Ba, O, C and Al; (b) depth profile of S, Mg, Ti, N and Si; (c) depth profile of Na; (c) depth profile of Cl; for the reference sample, sample exposed for 40 days, and the sample exposed for 120 days.

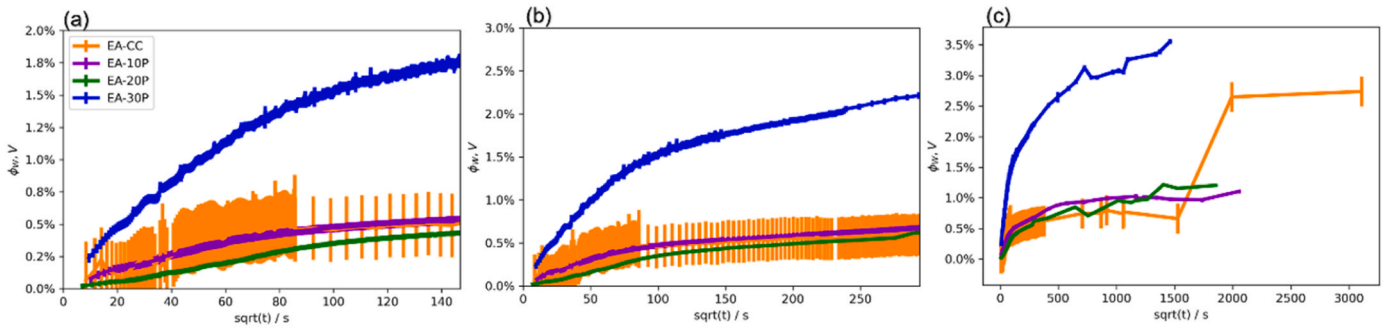

Fig. 11. Volumetric water uptake ($\varnothing_w, V$) calculated using linear relationship during (a) the first 6 h of exposure, (b) 24 h, and (c) the course of the measurement.

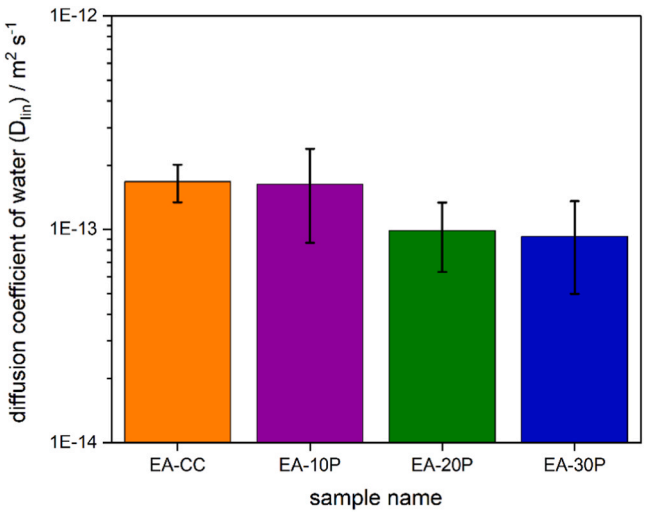

Fig. 12. Values of diffusion coefficient on volumetric water uptake evolution calculated using linear relationship (**D_lin**) for different coatings.

pigmented coating became significant with increase in the aging temperature, due to the stress built-up and resulting larger variability of diffusion pathways [9]. Therefore, although in EA-CC, the pseudo-Fickian diffusion may be due to the partial plasticization and/or decrease in the available polar groups, addition of pigments expands the non-Fickian section most likely by increasing the distribution of diffusion process (diffusion pathways and/or diffusion constant) and stress built-up.

3.4. Investigating ion diffusion mechanism

A common approach to investigate the nature of the diffusion of liquids and solvents in polymers is to study the movement of the diffusion front. Using the two-layer model, the position of the ions diffusion front along the thickness could be monitored by subtracting the thickness of the inner layer as the ion free zone from the thickness of the coating at each time spot. The evolution of the front versus square root of time is illustrated in Fig. 13.a. EA-20P and EA-30P show a linear behaviour with regard to the square root of time. This behaviour characterizes a Fickian diffusion of ions, all throughout the depth of the coating [56]. In EA-10P, only the initial part follows a linear function with $t^{0.5}$. After around 70 h (purple dashed line in Fig. 13), the interpretation of the parameter d changes and this parameter represents the thickness of the inner layer of the coating with different morphology. For EA-CC, Fickian behaviour is dominant during the first 31.7 h (orange dashed line in Fig. 13). Hereafter, the movement of the front slows down.

The correlation between the ingress front and the square root of time is shown in Eq. 5. The value of A for the samples shown in Fig. 13 is written inside the figure while the average value for 3 samples is compared in Fig. 13.b.

$$\lambda_{d_p} = At^{0.5} \tag{5}$$

When comparing EA-20P and EA-30P that both follow a Fickian regime, ions penetrate significantly faster in EA-30P with higher PVC. As shown in Fig. 7, λ has also higher value in EA-30P, showing higher concentration of ions in this coating which was confirmed in GDOES depth profiles. Comparison among EA-20P/EA-30P and EA-10P is not as straightforward, and A could only be computed for the first 70 h. However, in comparison to EA-CC, ion diffusion is significantly promoted in pigmented coatings. It's noteworthy that although the diffusion mechanism of water in EA-30P and EA-20P deviated from Fickian after around 2 h, the diffusion of ions is happening through a Fickian regime till they approach the buried interface. This confirms the independent transport behaviour of the hydrated ions in comparison to water in these pigmented coatings. The diffusion of ions can happen through the preferential paths formed due to the incorporation of the pigments, such as the pigment/polymer interphase.

4. Conclusions

It was shown that the two-layer EEC model is a powerful tool in providing information about the morphological/structural induced electrochemical response of the coated structures. As such, the movement of the ions diffusion front in different coatings was investigated in correlation to the coating's morphology/structure. It was found that in coatings with distinct layered structure as illustrated by GDOES depth profiles and SEM images, the resistivity distribution originating from structural heterogeneities could dominate the influence of penetrating ions on the resistivity profile. In such samples, e.g., EA-10P, the two-layer model is limited in following the penetration of ions and rather models the bi-layer like structure of the coating after certain time. In more homogeneous coatings (EA-20P and EA-30P), the influence of diffusing ions dominates the resistivity profile. Hence, the diffusion of ions could be monitored all along thickness towards the buried interface. Furthermore, mechanistic insights were provided regarding the electrolyte transport which evidenced the different mechanism of ion diffusion with respect to the mechanism of water diffusion. Apart from

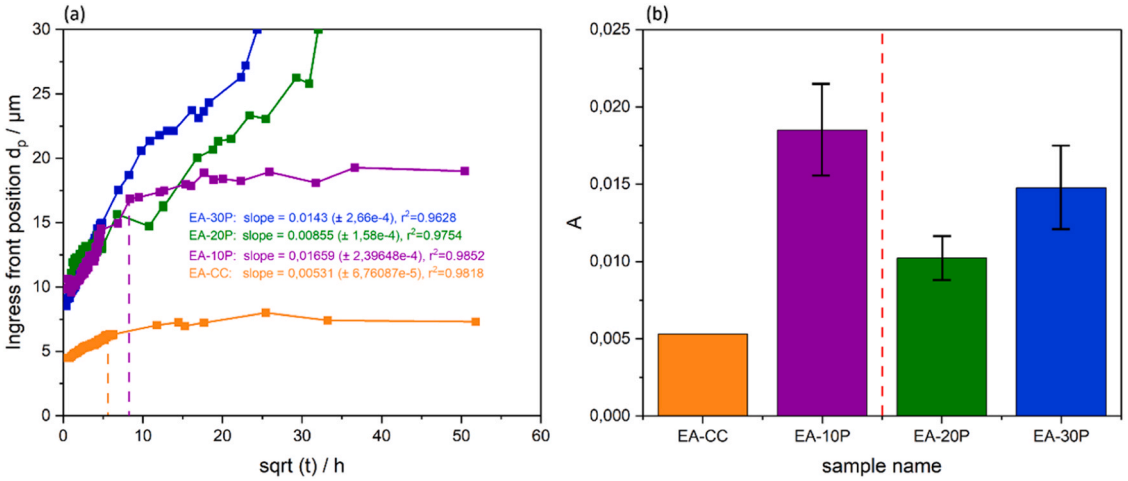

Fig. 13. (a): The evolution of the ingress front as a function of the square root of time; (b) The comparison between the value of the parameter A as in Eq. 5.

EA-10P, among the EA-CC, EA-20P, and EA-30P, faster ion diffusion and promoted water uptake was outlined with increase in PVC. Besides ORP-EIS, GDOES could also successfully reveal the depth profile of the ions diffusing from the electrolyte in EA-CC and EA-30P. While GDOES could potentially provide information on the depth profile of the diffusing ions in EA-10P and EA-20P, presence of ions in the pigment's composition introduced restrictions to the systems under the study. Additionally, the combination of GDOES and SEM imaging was proved useful in generating information on the morphology/structure of the coatings to correlate with ORP-EIS results.

CRediT authorship contribution statement

Negin Madelat: Conceptualization, Methodology, Investigation, Validation, Formal analysis, Writing – original draft. **Benny Wouters**: Methodology, Software, Formal Analysis, Writing – review & editing. **Peter Visser**: Resources, Methodology, Investigation, Writing – review & editing. **Zahra Jiryaeisharahi**: Investigation, Validation. **Kristof Marcoen:** Investigation, Validation. **Shoshan T. Abrahami:** Investigation, Validation. **Annick Hubin**: Funding acquisition, Conceptualization, Methodology. **Herman Terryn**: Funding acquisition, Project administration, Methodology, Writing – review & editing. **Tom Hauffman**: Funding acquisition, Supervision, Methodology, Writing – review & editing.

Declaration of Competing Interest

The authors declare that they have no known competing financial interests or personal relationships that could have appeared to influence the work reported in this paper.

Data availability

The raw/processed data required to reproduce these findings cannot be shared at this time as the data also forms part of an ongoing study.

Acknowledgements

This research is funded by the SBO project PredictCor (project number: FWOSBO22) of the Research Foundation – Flanders (FWO). Special thanks go to OCAS for their help with GDOES measurements and Priya Laha from Vrije Universiteit Brussel for SEM measurements.

References

[1] P.A. Sørensen, S. Kiil, K. Dam-Johansen, C.E. Weinell, Anticorrosive coatings: a review, J. Coat. Technol. Res. 6 (2009) 135–176, https://doi.org/10.1007/s11998-008-9144-2.
[2] M.F. Montemor, Functional and smart coatings for corrosion protection: a review of recent advances, Surf. Coat. Technol. 258 (2014) 17–37, https://doi.org/10.1016/j.surfcoat.2014.06.031.
[3] D.Y. Perera, Effect of pigmentation on organic coating characteristics 50 (2004) 247–262, https://doi.org/10.1016/j.porgcoat.2004.03.002.
[4] G.K. Van Der Wel, O.C.G. Adan, Moisture in organic coatings - a review, Prog. Org. Coat. 37 (1999) 1–14, https://doi.org/10.1016/S0300-9440(99)00058-2.
[5] S. Morsch, S. Lyon, P. Greensmith, S.D. Smith, S.R. Gibbon, Water transport in an epoxy-phenolic coating, Prog. Org. Coat. 78 (2015) 293–299, https://doi.org/10.1016/j.porgcoat.2014.08.006.
[6] S. Morsch, S. Lyon, S.D. Smith, S.R. Gibbon, Mapping water uptake in an epoxy-phenolic coating, Prog. Org. Coat. 86 (2015) 173–180, https://doi.org/10.1016/j.porgcoat.2015.05.017.
[7] S.G.R. Emad, X. Zhou, S.B. Lyon, G.E. Thompson, Y. Liu, G. Smyth, D. Graham, D. Francis, S.R. Gibbon, Influence of volume concentration of active inhibitor on microstructure and leaching behaviour of a model primer, Prog. Org. Coat. 102 (2017) 71–81, https://doi.org/10.1016/j.porgcoat.2016.04.039.
[8] F. Meng, L. Liu, W. Tian, H. Wu, Y. Li, T. Zhang, F. Wang, The influence of the chemically bonded interface between fillers and binder on the failure behaviour of an epoxy coating under marine alternating hydrostatic pressure, Eval. Program Plann. (2015), https://doi.org/10.1016/j.corsci.2015.09.011.
[9] C. Vosgien Lacombre, D. Trinh, G. Bouvet, X. Feaugas, S. Mallarino, S. Touzain, Influence of pigment on the degradation of anticorrosion polymer coatings using a thermodynamic analysis of electrochemical impedance spectroscopy data, Electrochim. Acta 234 (2017) 7–15, https://doi.org/10.1016/j.electacta.2017.03.050.
[10] C. Vosgien Lacombre, G. Bouvet, D. Trinh, X. Feaugas, S. Touzain, S. Mallarino, Influence of pigment and internal stresses on water uptake in model epoxy: a thermodynamic approach, J. Mater. Sci. 53 (2018) 2253–2267, https://doi.org/10.1007/s10853-017-1647-8.
[11] C. Vosgien Lacombre, G. Bouvet, D. Trinh, S. Mallarino, S. Touzain, Effect of pigment and temperature onto swelling and water uptake during organic coating ageing, Prog. Org. Coat. 124 (2018) 249–255, https://doi.org/10.1016/j.porgcoat.2017.11.022.
[12] S. Morsch, S. Emad, S.B. Lyon, S.R. Gibbon, M. Irwin, Progress in organic coatings the location of adsorbed water in pigmented epoxy-amine coatings, Prog. Org. Coat. 173 (2022), 107223, https://doi.org/10.1016/j.porgcoat.2022.107223.
[13] J.J. Gracenea, J.J. Saura, J.J. Suay, The influence of the critical pigment volume concentration (CPVC) on the properties of an epoxy coating Part II. Anticorrosion and economic properties, c (2004) 68–74. https://doi.org/10.1016/j.porgcoat.2003.10.014.
[14] N. PEBERE, T. PICAUD, M. DUPRAT, F. DABOSI, Evaluation of corrosion performance of coated steel by the impedance technique, Corros. Sci. 29 (1989) 1073–1086, https://doi.org/10.1016/0010-938X(89)90045-0.
[15] U. Rammelt, G. Reinhard, Application of electrochemical impedance spectroscopy (EIS) for characterizing the corrosion-protective performance of organic coatings on metals, Prog. Org. Coat. 21 (1992) 205–226, https://doi.org/10.1016/0033-0655(92)87005-U.
[16] F. Mansfeld, Use of electrochemical impedance spectroscopy for the study of corrosion protection by polymer coatings, J. Appl. Electrochem. 25 (1995) 187–202, https://doi.org/10.1007/BF00262955.
[17] A. Amirudin, D. Thieny, Application of electrochemical impedance spectroscopy to study the degradation of polymer-coated metals, Prog. Org. Coat. 26 (1995) 1–28, https://doi.org/10.1016/0300-9440(95)00581-1.
[18] A. Lasia, Electrochem. impedance Spectrosc. its Appl. (2014), https://doi.org/10.1007/978-1-4614-8933-7.
[19] P. Margarit, Electrochimica Acta EIS and organic coatings performance: revisiting some key points, Electrochim. Acta 354 (2020), 136725, https://doi.org/10.1016/j.electacta.2020.136725.
[20] D.H. Xia, C.M. Deng, D. Macdonald, S. Jamali, D. Mills, J.L. Luo, M.G. Strebl, M. Amiri, W. Jin, S. Song, W. Hu, Electrochemical measurements used for assessment of corrosion and protection of metallic materials in the field: a critical review, J. Mater. Sci. Technol. 112 (2022) 151–183, https://doi.org/10.1016/j.jmst.2021.11.004.
[21] T. Breugelmans, E. Tourwé, J.B. Jorcin, A. Alvarez-Pampliega, B. Geboes, H. Terryn, A. Hubin, Odd random phase multisine EIS for organic coating analysis, Prog. Org. Coat. 69 (2010) 215–218, https://doi.org/10.1016/j.porgcoat.2010.04.008.
[22] M. Meeusen, P. Visser, L. Fernández Macía, A. Hubin, H. Terryn, J.M.C. Mol, The use of odd random phase electrochemical impedance spectroscopy to study lithium-based corrosion inhibition by active protective coatings, Electrochim. Acta 278 (2018) 363–373, https://doi.org/10.1016/j.electacta.2018.05.036.
[23] B. Wouters, E. Jalilian, R. Claessens, N. Madelat, T. Hauffman, G. Van Assche, H. Terryn, A. Hubin, Monitoring initial contact of UV-cured organic coatings with aqueous solutions using odd random phase multisine electrochemical impedance spectroscopy, Corros. Sci. 190 (2021), 109713, https://doi.org/10.1016/j.corsci.2021.109713.
[24] M.A. Jedrzejczyk, N. Madelat, B. Wouters, H. Smeets, M. Wolters, S.A. Stepanova, T. Vangeel, K. Van Aelst, S. Van den Bosch, J. Van Aelst, V. Polizzi, K. Servaes, K. Vanbroekhoven, B. Lagrain, B.F. Sels, H. Terryn, K.V. Bernaerts, Preparation of renewable thiol-Yne "Click" networks based on fractionated lignin for anticorrosive protective film applications, Macromol. Chem. Phys. 223 (2022), https://doi.org/10.1002/macp.202100461.
[25] N. Madelat, B. Wouters, E. Jalilian, G. Van Assche, A. Hubin, H. Terryn, T. Hauffman, Differentiating between the diffusion of water and ions from aqueous electrolytes in organic coatings using an integrated spectro-electrochemical technique, Corros. Sci. 212 (2023), 110919, https://doi.org/10.1016/j.corsci.2022.110919.
[26] M. Meeusen, J.P.B. van Dam, N. Madelat, E. Jalilian, B. Wouters, T. Hauffman, G. Van Assche, J.M.C. Mol, A. Hubin, H. Terryn, FEM modelling to predict spatiotemporally resolved water uptake in organic coatings: experimental validation by odd random phase electrochemical impedance spectroscopy measurements, Prog. Org. Coat. 182 (2023), 107710, https://doi.org/10.1016/j.porgcoat.2023.107710.
[27] S. Pletincx, J.M.C. Mol, H. Terryn, A. Hubin, T. Hauffman, An in situ spectro-electrochemical monitoring of aqueous effects on polymer/metal oxide interfaces, J. Electroanal. Chem. 848 (2019), 113311, https://doi.org/10.1016/j.jelechem.2019.113311.
[28] N. Madelat, B. Wouters, Z. Jiryaeisharahi, A. Hubin, H. Terryn, T. Hauffman, An ORP-EIS approach to distinguish the contribution of the buried interface to the electrochemical behaviour of coated aluminium, Electrochim. Acta 455 (2023), 142400, https://doi.org/10.1016/j.electacta.2023.142400.
[29] X. Zhu, N. Hallemans, B. Wouters, R. Claessens, J. Lataire, A. Hubin, Operando odd random phase electrochemical impedance spectroscopy as a promising tool for monitoring lithium-ion batteries during fast charging, J. Power Sources 544 (2022), 231852, https://doi.org/10.1016/j.jpowsour.2022.231852.
[30] T. Collet, N. Hallemans, B. Wouters, K. Ramharter, J. Lataire, R. Pintelon, A. Hubin, An operando ORP-EIS study of the copper reduction reaction supported by thiourea and chlorides as electrorefining additives, Electrochim. Acta 389 (2021), 138762, https://doi.org/10.1016/j.electacta.2021.138762.

[31] E. Van Gheem, R. Pintelon, J. Vereecken, J. Schoukens, A. Hubin, P. Verboven, O. Blajiev, Electrochemical impedance spectroscopy in the presence of non-linear distortions and non-stationary behaviour, Part I: Theory Valid., Electrochim. Acta 49 (2004) 4753–4762, https://doi.org/10.1016/j.electacta.2004.05.039.
[32] E. Van Gheem, R. Pintelon, A. Hubin, J. Schoukens, P. Verboven, O. Blajiev, J. Vereecken, Electrochemical impedance spectroscopy in the presence of non-linear distortions and non-stationary behaviour: Part II. Application to crystallographic pitting corrosion of aluminium, Electrochim. Acta 51 (2006) 1443–1452, https://doi.org/10.1016/j.electacta.2005.02.096.
[33] Y. Van Ingelgem, E. Tourwé, O. Blajiev, R. Pintelon, A. Hubin, Advantages of odd random phase multisine electrochemical impedance measurements, Electroanalysis 21 (2009) 730–739, https://doi.org/10.1002/elan.200804471.
[34] T. Breugelmans, An identification approach as a prerequisite for quantitative electrochemical studies - PhD Thesis, 2010.
[35] T. Breugelmans, J. Lataire, T. Muselle, E. Tourwé, R. Pintelon, A. Hubin, Odd random phase multisine electrochemical impedance spectroscopy to quantify a non-stationary behaviour: Theory and validation by calculating an instantaneous impedance value, Electrochim. Acta 76 (2012) 375–382, https://doi.org/10.1016/j.electacta.2012.05.051.
[36] A.S. Nguyen, M. Musiani, M.E. Orazem, N. Pébère, B. Tribollet, V. Vivier, Impedance analysis of the distributed resistivity of coatings in dry and wet conditions, Electrochim. Acta 179 (2015) 452–459, https://doi.org/10.1016/j.electacta.2015.02.109.
[37] A.S. Nguyen, M. Musiani, M.E. Orazem, N. Pébère, B. Tribollet, V. Vivier, Impedance study of the influence of chromates on the properties of waterborne coatings deposited on 2024 aluminium alloy, Corros. Sci. 109 (2016) 174–181, https://doi.org/10.1016/j.corsci.2016.03.030.
[38] A.S. Nguyen, N. Causse, M. Musiani, M.E. Orazem, N. Pébère, B. Tribollet, V. Vivier, Determination of water uptake in organic coatings deposited on 2024 aluminium alloy: Comparison between impedance measurements and gravimetry, Prog. Org. Coat. 112 (2017) 93–100, https://doi.org/10.1016/j.porgcoat.2017.07.004.
[39] Y. Chen, A. Son, M.E. Orazem, B. Tribollet, N. Pébère, M. Musiani, V. Vivier, Electrochimica acta identification of resistivity distributions in dielectric layers by measurement model analysis of impedance spectroscopy, Electrochim. Acta 219 (2016) 312–320, https://doi.org/10.1016/j.electacta.2016.09.136.
[40] L. Young, Anodic oxide films, Trans. Faraday Soc. 51 (1955) 1250–1260, https://doi.org/10.1524/zpch.1963.39.5_6.405.
[41] H. Göhr, Über Beiträge einzelner Elektrodenprozesse zur Impedanz, Ber. Der Bunsenges. Für Phys. Chem. 85 (1981) 274–280, https://doi.org/10.1002/bbpc.19810850405.
[42] H. Göhr, J. Schaller, C.A. Schiller, Impedance studies of the oxide layer on zircaloy after previous oxidation in water vapour at 400°C, Electrochim. Acta 38 (1993) 1961–1964, https://doi.org/10.1016/0013-4686(93)80323-R.
[43] B. Hirschorn, M.E. Orazem, B. Tribollet, V. Vivier, I. Frateur, M. Musiani, Determination of effective capacitance and film thickness from constant-phase-element parameters, Electrochim. Acta 55 (2010) 6218–6227, https://doi.org/10.1016/j.electacta.2009.10.065.
[44] A.S. Castela, A.M. Simões, Water sorption in freestanding PVC films by capacitance measurements, Prog. Org. Coat. 46 (2003) 130–134, https://doi.org/10.1016/S0300-9440(02)00220-5.
[45] D.M. Brasher, A.H. Kingsbury, Electrical measurements in the study of immersed paint coatings on metal. I. Comparison between capacitance and gravimetric methods of estimating water-uptake, J. Appl. Chem. 4 (1954) 62–72, https://doi.org/10.1002/jctb.5010040202.
[46] A.S. Castela, A.M. Simões, Assessment of water uptake in coil coatings by capacitance measurements, Prog. Org. Coat. 46 (2003) 55–61, https://doi.org/10.1016/S0300-9440(02)00190-X.
[47] L. Yung, Anodic Oxide Films, Academic Press,, New York, 1961, https://doi.org/10.1524/zpch.1963.39.5_6.405.
[48] V.B. Miskovic-Stankovic, M.D. Maksimović, Z. Kačarević-Popović, J.B. Zotović, The sorption characteristics and thermal stability of epoxy coatings electrodeposited on steel and steel electrochemically modified by Fe-P alloys, Prog. Org. Coat. 33 (1998) 68–75, https://doi.org/10.1016/S0300-9440(98)00011-3.
[49] Z.Ž. Lazarević, V.B. Mišković-Stanković, Z. Kačarević-Popović, D.M. Dražić, Determination of the protective properties of electrodeposited organic epoxy coatings on aluminium and modified aluminium surfaces, Corros. Sci. 47 (2005) 823–834, https://doi.org/10.1016/j.corsci.2004.07.016.
[50] M. SUN, F. LIU, H. SHI, E. HAN, A study on water absorption in freestanding polyurethane films filled with nano-TiO2 pigments by capacitance measurements, Acta Metall. Sin. (Engl. Lett. 22 (2009) 27–34, https://doi.org/10.1016/S1006-7191(08)60067-8.
[51] A.S. Castela, A.M. Simoes, An impedance model for the estimation of water absorption in organic coatings. Part I: a linear dielectric mixture equation, Corros. Sci. 45 (2003) 1631–1646, https://doi.org/10.1016/S0010-938X(03)00014-3.
[52] B. Efron, R. Tibshirani, An introduction to bootstrap, Chapman & Hall/CRC, 1994.
[53] F. Geenen, Characterisation of Organic Coatings with Impedance Spectroscopy, Ph. D. Thesis, 1991.
[54] M.M. Wind, H.J.W. Lenderink, A capacitance study of pseudo-fickian diffusion in glassy polymer coatings, Prog. Org. Coat. 28 (1996) 239–250, https://doi.org/10.1016/0300-9440(95)00601-X.
[55] A. Roggero, N. Caussé, E. Dantras, L. Villareal, A. Santos, N. Pébère, Thermal activation of impedance measurements on an epoxy coating for the corrosion protection: 2. electrochemical impedance spectroscopy study, Electrochim. Acta 305 (2019) 116–124, https://doi.org/10.1016/j.electacta.2019.03.007.
[56] H.L. Frisch, S.Alexander Stern, Diffusion of small molecules in polymers, Crit. Rev. Solid State Mater. Sci. 11 (1983) 123–187, https://doi.org/10.1080/01611598308244062.